View Online / Journal Homepage / Table of Contents for this issue
Dynamic Article Links

Soft Matter

Cite this: *Soft Matter*, 2012, **8**, 1817

www.rsc.org/softmatter

PAPER

Extreme water repellency of nanostructured low-surface-energy non-woven fabrics

Bongsu Shin,[a] Kwang-Ryeol Lee,[b] Myoung-Woon Moon*[b] and Ho-Young Kim*[a]

Received 30th September 2011, Accepted 11th November 2011
DOI: 10.1039/c1sm06867a

We report the extreme water repellent nature of non-woven fabrics of PET (polyethyleneterephthalate) whose fiber surfaces are nanotextured with oxygen plasma and coated with a low-surface-energy nanofilm. The surface effectively suppresses vapor condensation and repels condensed water droplets in addition to exhibiting a high contact angle and a low contact angle hysteresis with a millimetre-sized water drop. We also show that the surface maintains its superhydrophobicity after water-vapor condensation and after oil-wetting due to high-aspect-ratio nanohairs on the fibers. The superior water-repellent ability of the plasma treated non-woven fabric can be exploited in a variety of industrial applications including water harvesting and fuel cell water management even under oily contaminations.

1. Introduction

There have been numerous studies on super-water-repellent surfaces to date. Although the majority of the research effort has been directed towards the creation of roughness either on the microscale[1–8] or nanoscale[5–17] to impose superhydrophobicity on flat substrates since the work of Onda *et al.*,[18] the early water repellency technology of the mid-20th century mainly concerned the modification of textiles rather than flat surfaces.[19–21] Textiles, either woven or non-woven, are still widely used not only as clothes but also as industrial materials including filters, oil absorption fabrics, hygiene items, and geotextiles.[22] It has been known that simply lowering the surface energy of polymeric fibers, such as PET (polyethyleneterephthalate), cellulose, polyester and nylon, renders the textiles superhydrophobic.[23–28] As the roughness of the textiles, determined by the diameter of the fibers, is usually of the order of tens or hundreds of micrometres, some efforts have been made to develop smaller scale structures on the fabric surface to further increase hydrophobicity.[19–21] It was also reported that nanostructured fabric networks exhibit oleophilicity, suggesting an interesting possibility to use the material for oil recovery and oil–water separation.[29,30]

Superhydrophobicity has been commonly characterized by the high contact angle of a surface with a (usually millimetre-sized) water drop approaching 180° and the low substrate tilt angle for the onset of drop rolling. However, additional measures of the quality of superhydrophobicity have recently attracted attention.[31–37] Lafuma and Quéré[31] pointed out that a robust superhydrophobic surface should be able to sustain a high contact angle against increased interior pressure of the drop (that may be caused by squeezing the drop between plates or by reducing the drop size). The work by Cheng *et al.*[32] called attention to the importance of superhydrophobic robustness against vapor condensation by showing that the lotus leaf, with a natural superhydrophobic surface, loses its hydrophobicity after water vapor condenses on its surface.

In this work, we develop an extreme water repellent surface with a surface-treatment method to induce nanoscale roughness on non-woven fabric (NWF) of PET and to lower its surface energy using the plasma enhanced chemical vapor deposition (PECVD) technique. This technique is advantageous because it can quickly generate superhydrophobic structures on a large surface area without the aid of photolithography and the aspect ratio (AR) of nanostructures can be controlled only by changing the plasma treatment duration.[10,24–27,38–43] Upon showing the superior water repellency (from a conventional perspective) of thus-prepared NWF by measuring the contact angle and the contact angle hysteresis (CAH) of the surface with a millimetre-sized water drop, we further investigate the robustness of superhydrophobicity of the surface. By observing the condensation of water drops of submicrometres in radius, we assess the hydrophobicity under increased interior pressure of the drop and the ability to prevent water flooding inside the fabric network. We then measure the contact angle of a millimetre-sized water drop on NWF that has gone through vapor condensation to evaluate the ability to sustain water repellency after condensation. Furthermore, we investigate the effects of the AR of nanohairs on NWF upon the ability to sustain water repellency after deposition of low-surface-energy liquids such as hexane, decane, octane and silicone oil.

[a]*School of Mechanical and Aerospace Engineering, Seoul National University, 151-744 Seoul, Korea. E-mail: hyk@snu.ac.kr; Fax: +82-2-880-9287; Tel: +82-2-880-9286*
[b]*Future Convergence Research Division, Korea Institute of Science and Technology, 136-791 Seoul, Korea. E-mail: mwmoon@kist.re.kr; Tel: +82-2-956-5498*

2. Experimental

Preparation of the superhydrophobic NWF surface

We started with a commercially available NWF (LG Chemical) of PET. As shown in Fig. 1(a), we formed nanohair structures on each fabric fiber surface by oxygen plasma etching and then coated the surface with a low-surface-energy material using a radio frequency-plasma enhanced chemical vapor deposition (rf-PECVD) technique. In the oxygen plasma etching, the duration was varied from 1 min to 60 min at a bias voltage of −400 V. It was found that below the bias voltage of −200 V, the nanohair structures were hardly formed due to low plasma power, while above −600 V, the etching rate of polymer was too high to obtain high AR nanohairs. The operating pressure and flow rate were kept at 10 mTorr and 20 cm^3 min^{-1}, respectively. The resulting hydrophilic surface with nanoscale roughness was hydrophobized with a coating of HMDSO (hexamethyldisiloxane, Sigma Aldrich) having the surface energy of 24.4 mJ m^{-2}. The HMDSO precursor gas was decomposed and its hydrophobic functional group was coated at the bias voltage of −400 V, the pressure of 4 mTorr, and the flow rate of 20 cm^3 min^{-1} for 30 s, resulting in SiO_x–C:H film. The growth rate of the SiO_x–C:H film on a flat Si wafer was measured to be 0.7 nm s^{-1} *via* an independent experiment with an atomic force microscope (AFM, Park Systems, XE-100), thus we speculate that approximately 20 nm-thick SiO_x–C:H film was grown on the polymer surface as well. In addition to NWF, the identical surface treatment was carried out on flat PET surfaces to compare their water repellent characteristics.

SEM image analysis and contact angle measurement

The nanostructures formed on NWF were imaged with a SEM (scanning electron microscope, FEI, Nova NanoSEM 200). Prior to observation, 10 nm-thick Pt film was coated on the samples.

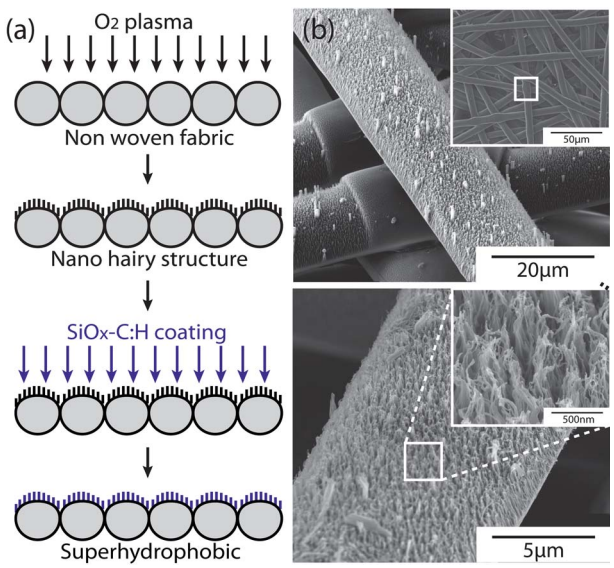

Fig. 1 (a) A schematic of nano-texturing and hydrophobic coating on NWF using PECVD. (b) SEM images of surface morphology of a nanotextured NWF etched by oxygen plasma for 60 min.

An electron accelerating voltage was 10 kV. Both the top and tilted views of the surfaces were imaged to measure the AR (a ratio of the height to the diameter) of nanohairs on the surface. The contact angle of water on the surfaces was measured using sessile DI (deionized) water droplets of 5 μl in volume with a goniometer (Kruss, DSA 100). In addition to the static contact angle, the critical advancing (receding) contact angle was measured by increasing (decreasing) the drop volume with an aid of a syringe needle immersed in the drop until the contact line starts to move. The difference between the critical advancing and receding contact angles corresponds to the CAH.

Water condensation experiment in ESEM

Heterogeneous nucleation and subsequent condensation process of water droplets on solid surfaces were observed with an ESEM (environmental scanning electron microscope, FEI XL-30 FEG). As the substrates, we used a superhydrophilic NWF (etched by oxygen plasma for 30 min) and a superhydrophobic NWF (etched by oxygen plasma for 60 min and coated with SiO_x–C:H for 30 s). The substrate temperature was maintained at 275 K by a cold stage module. The initial chamber pressure was below the saturation pressure of water vapor at 275 K (5.2 Torr) and was gradually increased to induce water nucleation on the surfaces. The surface images were taken every 10 s.

Post-condensation wetting behavior

We measured the contact angle of water droplets on a surface on which vapor condensation had taken place. To this end, we first placed vertically three different kinds of surfaces (pristine NWF, superhydrophobic flat PET, and superhydrophobic NWF) in an acrylic chamber where the surface temperature and the relative humidity of the surrounding air were kept at 2 °C and 100%, respectively. The surface temperature increased to approximately 10 °C during the experiment. To induce superhydrophobicity, the surfaces were etched with oxygen plasma for 60 min and coated with SiO_x–C:H for 30 s. After going through vapor condensation for 10 min, the surfaces were horizontally placed in an atmospheric environment (temperature 20 °C and humidity ~50%). The water droplets of 5 μl in volume were deposited on the surfaces to measure the contact angles.

Wetting behavior after low-surface-energy liquid deposition

We first wet surfaces of NWF (pristine and superhydrophobic) of 2 cm × 2 cm in area with liquids of low surface energy, such as hexane, decane, octane and silicone oil, whose properties are listed in Table 1. The liquids were dyed with 1 vol% of blue-colored ink to distinguish them from transparent water droplets.

Table 1 Surface energy and kinematic viscosity of the low-surface-energy liquids at 20 °C

Liquid	Surface energy (mN m^{-1})	Kinematic viscosity (mm^2 s^{-1})
Hexane	18.4	0.51
Octane	21.6	0.805
Decane	23.8	1.26
Silicone oil	21.2	1000

When NWFs were pre-wet by volatile hydrocarbons (hexane, decane and octane), the contact angle of water on NWFs was measured within 5 s after pre-wetting. When silicone oil was used for pre-wetting which took a considerable time to spread out due to its high viscosity, the contact angle of water was measured twice at 1 and 24 h after pre-wetting. We also measured the contact angle of a water drop of 5 μl in volume on liquid films of the low-surface-energy hexane and silicone oil independently.

3. Results and discussion

3.1 Surface morphology

As shown in Fig. 1(b), nanohair structures are formed on the plasma-irradiated regions of randomly distributed NWF. We plot the average AR of at least 20 nanohairs *versus* the plasma treatment duration in Fig. 2(a). For short durations from 1 to 5 min, AR is close to unity. As the plasma treatment duration exceeds 10 min, AR increases dramatically from approximately 4 (10 min) to 50 (60 min).

The NWF consists of threads of PET whose molecular formula is $(C_{10}H_8O_4)_n$. The oxygen plasma cuts the link of carbon, hydrogen and oxygen quite efficiently thus has a high etching rate. Polymer chains containing oxygen are known to form a nanofibrillar structure by oxygen plasma through dewetting.[44] Consequently, for longer duration of oxygen plasma treatment, higher AR for nanofibrils or nanohairs can be achieved on the surface of the NWFs. It is noted that the chemical structure of PET in the modified NWF tends to change, so that C–O bonds (methylene carbon atoms singly bonded to oxygen) and O═C–O bonds (ester carbon atoms) are remarkably increased by oxygen plasma treatment due to the incorporation of oxygen into the PET surface.[42]

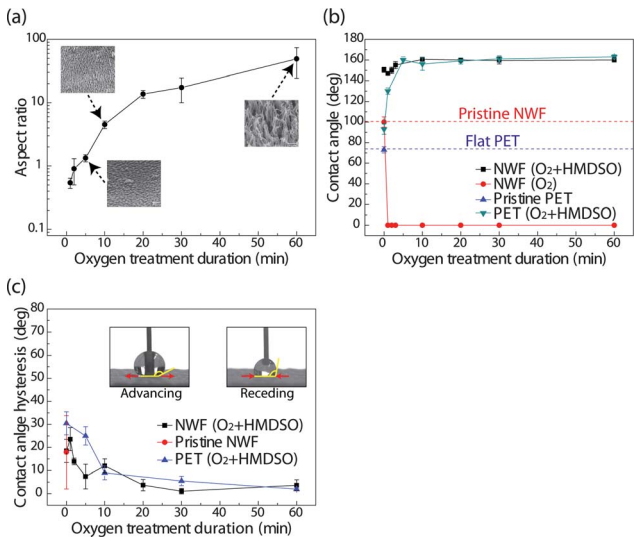

Fig. 2 Measurement results of (a) aspect ratio of nanohairs, (b) contact angle of a water drop and (c) contact angle hysteresis of a water drop on the superhydrophobic NWF and the superhydrophobic flat PET substrate *versus* oxygen plasma treatment duration. The SiO_x–C:H coating duration is uniformly 30 s. Insets of (c) show the measurement scheme of the advancing and the receding contact angle.

3.2 Contact angle of a sessile water drop on dry surfaces

Fig. 2(b–c) shows the measurement results of the static contact angle and CAH of sessile water drops on various dry surfaces. The flat surface of PET has a static contact angle of 73° ± 3°, revealing its slightly hydrophilic nature. The NWF, an entangled structure of PET threads with tens of micrometres in diameter, has an increased contact angle of 100° ± 5° owing to the microscale roughness. Upon the oxygen plasma etching, the NWF surface becomes superhydrophilic regardless of plasma irradiation duration because it corresponds to the high-surface-energy chemical modification. As the hydrophobic SiO_x–C:H film was deposited to reduce the surface energy, the static contact angles (and CAH) on a flat PET surface and an NWF surface not treated by oxygen plasma were measured to be 93° ± 5° (31° ± 5°) and 151° ± 3° (19° ± 5°), respectively. The high contact angle and a low CAH of the SiO_x–C:H film coated NWF (without etching) indicates that merely hydrophobizing microthreads can impose strong water repellency on NWF to an extent.

However, it is seen that oxygen plasma treatment longer than 10 min, which creates nanohairs of a high AR on the surfaces, further increases the static contact angle and greatly reduces CAH for both flat PET and NWF. The static contact angle reaches 163° ± 2° and 160° ± 2° for flat PET and NWF with 60 min of the oxygen plasma treatment and 30 s of SiO_x–C:H coating. The minimum CAH attainable by the oxygen plasma treatment and SiO_x–C:H coating is 1° for NWF (30 min plasma treatment) and 2° for flat PET (60 min plasma treatment). These results show that oxygen plasma treatment and SiO_x–C:H coating can create super-water-repellent nanohair structures both on flat PET and NWF surfaces.

3.3 Water vapor condensation on NWF

Here we compare the condensation behavior of water on a superhydrophilic NWF (etched by oxygen plasma for 30 min) and on a superhydrophobic NWF (etched by oxygen plasma for 60 min and coated with SiO_x–C:H for 30 s) using the images taken by an ESEM. As shown in Fig. 3(a), filmwise condensation around fibers occurs on the superhydrophilic NWF under a super-saturation condition. The growing water film fills the interstitial spaces and eventually leads to flooding. On the other hand, as shown in Fig. 3(b), dropwise condensation occurs on the fibers of the superhydrophobic NWF. Upon nucleation, the water droplets grow and coalesce with neighboring droplets. The rate of nucleation is significantly lower than that on the superhydrophilic NWF, which can be

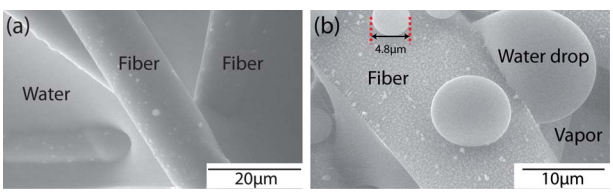

Fig. 3 ESEM images of condensation behavior of water vapor on the (a) superhydrophilic NWF and (b) superhydrophobic NWF. The vapor pressure in the chamber is 6.6 and 6.2 Torr in (a) and (b), respectively.

explained by the following Sigsbee's equation that gives the rate of heterogeneous nucleation as a function of the contact angle and the surface tension:[45]

$$J = J_0 \exp[-\pi\gamma r^{*2}(2 - 3\cos\theta + \cos^3\theta)/3kT] \quad (1)$$

where J is the nucleation rate, J_0 a kinetic constant, γ the liquid–vapor surface energy per unit area, r^* the critical radius, θ the equilibrium contact angle, k the Boltzmann constant and T the absolute temperature. It states that the nucleation rate sharply decreases with the increase of the contact angle. Owing to the low nucleation rate and the dropwise condensation of water on the superhydrophobic NWF, the interstitial space of the fiber network largely remains dry, implying that it can provide a passage for vapor flow even in wet environment. This aspect of strong water repellency can be beneficial in a variety of applications, including the water management of fuel cell membranes[46,47] and the fabrication of functional fabrics.[19,21,48,49]

The ability of ESEM to observe microscale water drops enables us to measure the robustness of the superhydrophobic surface against a high liquid pressure. The Young–Laplace equation relates the pressure difference (Δp) across the gas–liquid interface to the surface tension and the interface curvature:

$$\Delta p = \gamma\left(\frac{1}{R_1} + \frac{1}{R_2}\right) \quad (2)$$

where R_1 and R_2 are the principal radii of curvature. For a spherical-cap shaped sessile drop, $R_1 = R_2 = R$, thus we get $\Delta p = 2\gamma/R$. The small droplets formed and observed in the ESEM chamber allow us to measure the contact angle of water on a solid surface under a very high Laplace pressure (Δp). Although it is not easy to accurately measure the contact angle of droplets on fibers through ESEM images, we find that even the smallest droplet observable in the setup, having the radius of 2.4 μm, maintained the contact angle higher than 90°. This implies that the superhydrophobic NWF fiber with high AR nanohairs can maintain its hydrophobicity at least up to 62 kPa, which is much higher than the threshold pressure (the pressure over which the contact angle abruptly reduces below 90° because of the transition from the Cassie–Baxter state[50] to the Wenzel state[51]) of the superhydrophobic surfaces reported by other researchers.[8,37,52,53]

3.4 Post-condensation hydrophobicity

Fig. 4 shows the images of sessile water drops of 5 μl in volume placed on the pristine NWF (see Fig. 4(a)), the superhydrophobic flat PET substrate (4(b)), and the superhydrophobic NWF (4(c)), all of which went through condensation of vapor on the surfaces. Both the superhydrophobic flat PET substrate and the superhydrophobic NWF were etched by oxygen plasma for 60 min and coated with SiO_x–C:H for 30 s. In dry states, the surfaces had the contact angle as 105° (Fig. 4(a)), 165° (4(b)) and 162° (4(c)) as shown in the insets. It is seen that on the pristine NWF and the superhydrophobic flat PET, the post-condensation contact angles of water are greatly reduced as compared with those on dry surfaces: the contact angle on the pristine NWF and the superhydrophobic flat PET was reduced to 64° and 137°, respectively. However, the superhydrophobic NWF maintains a high contact angle (156°) even after condensation.

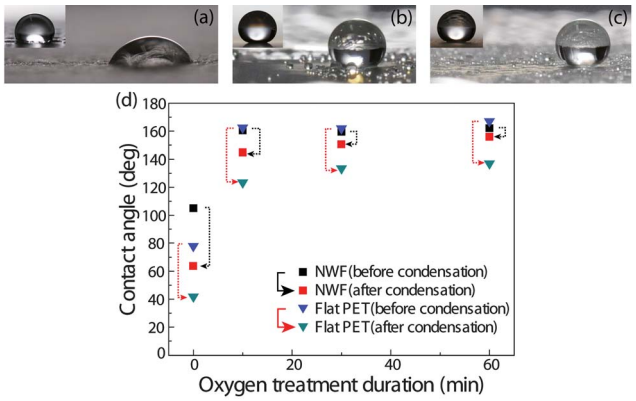

Fig. 4 The images of sessile water drops on (a) pristine NWF, (b) flat superhydrophobic PET, and (c) superhydrophobic NWF, all of which have gone through vapor condensation on their surfaces. The insets of each Fig. show the water drop deposited on dry surfaces. (d) The contact angle of water drops on the superhydrophobic NWF and the flat superhydrophobic PET substrate before and after condensation of water vapor *versus* the oxygen plasma treatment duration.

Fig. 4(d) quantitatively shows the change of the contact angle that is measured before and after vapor condensation for NWF and flat PET substrate depending on the oxygen plasma treatment duration. For pristine materials, both the NWF and the flat PET substrate show significant reduction of the contact angle (by approximately 40°) after vapor condensation. This implies that residual water on the surface after condensation facilitates the spreading of a newly added sessile drop. For the flat PET surfaces etched by oxygen plasma and coated with SiO_x–C:H, the contact angle in the dry state is very high (165°) but it decreases by about 37° when the oxygen treatment duration is 10 min. The amount of contact angle reduction decreases to about 26° when the oxygen treatment lasts 30 min or longer. On superhydrophobic NWF, the contact angle is reduced by 15°, 9° and 6° after condensation when the oxygen treatment lasts for 10 min, 30 min and 60 min, respectively. These results indicate the roles of microscale and nanoscale topographic features in suppressing the reduction of the contact angle after condensation: Microscale fibers of NWF play a dominant role in maintaining superhydrophobicity, and nanohairs (commonly existing on both flat PET substrate and NWF that are etched by oxygen plasma) tend to decrease the contact angle reduction as their AR increases.

Fig. 5 schematically illustrates the aforementioned roles of micro- and nano-scale features. In Fig. 5(a), water vapor and thus its nucleation sites are distributed over the surfaces of NWF fiber stacks. Hence, it is less likely that the entire surface is flooded with water due to condensation as also evidenced in the previous section. Moreover, large droplets formed by coalescence of tiny droplets tend to be squeezed out of interstices because they rather stay as spheres (having minimum surface area) on top of NWF than forming large contact area with water-repellent solid surfaces as trapped in interstices. In Fig. 5 (b), water droplets nucleated between nanohairs tend to be squeezed out for the same reason as above (to minimize the surface area contacting water-repellent solid surface). The

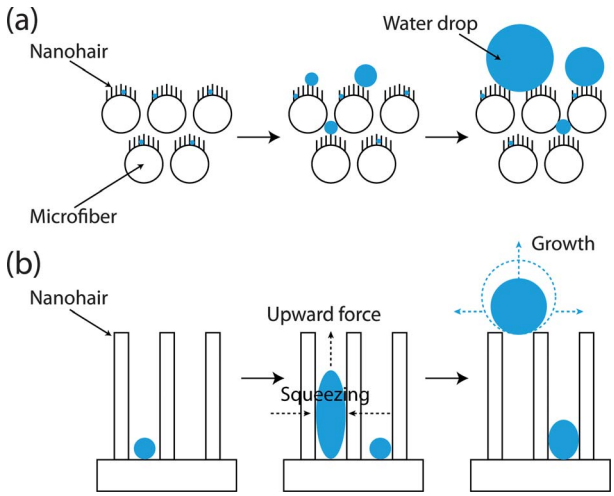

Fig. 5 Schematic of water repulsion behavior of (a) the superhydrophobic NWF and (b) the flat substrate with high aspect-ratio, hydrophobic nanohairs with small spacings.

higher the AR of the nanohairs, the more efficient is the separation of water droplets from basal area, which helps to prevent the transition from the Cassie–Baxter state to the Wenzel state.

3.5 Hydrophobicity after low-surface-energy liquid deposition

In this section, we investigate how the hydrophobicity of NWF is affected by pre-deposition of low-surface-energy liquids. A major reason that the NWF coated with SiO_x–C:H film has superhydrophobicity is that its surface has a lower surface energy (24.4 mJ m^{-2}) than that of water (71.7 mJ m^{-2}). However, hydrocarbons such as hexane, decane and octane have lower surface energy than SiO_x–C:H film as listed in Table 1. Consequently, NWFs with either single (microfiber network only) or dual (nanohair structures on microfiber network) roughness coated with SiO_x–C:H film exhibit superoleophilicity. Drops of all the three kinds of hydrocarbons with 40 μl in volume spread over the superhydrophobic NWF within a few seconds.

We start with hexane-deposited NWFs whose contact angle with water is shown in Fig. 6(a). It is recalled that the measurement of the contact angle of a water drop was performed within 5 s of the hydrocarbon deposition to eliminate the effect of hydrocarbon evaporation. On pristine NWF (no oxygen plasma treatment), the contact angle drops from 151° to 105° due to pre-wetting of hexane. This value is slightly larger than the contact angle of water on hexane film, 80°, implying that the hydrocarbon film separates a water droplet from the underlying NWF to an extent. With the increase of oxygen plasma treatment duration corresponding to the increase of the AR of nanohairs on the fibers of NWF, the contact angle of water increases. After deposition of small volumes (10 and 20 μl) of hexane, the contact angle of water is completely recovered to the value of dry NWF when the plasma treatment duration reaches 30 min (for 10 μl) and 60 min (for 20 μl). As the volume of hexane is increased to 40 μl, hydrophobicity of the NWF improves with the increase of the

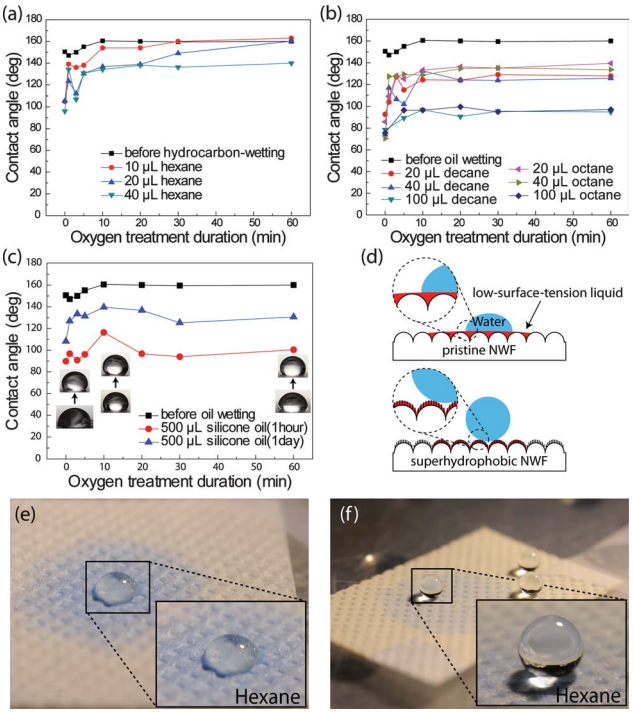

Fig. 6 Contact angle of a water drop on superhydrophobic-treated NWF after wetting of (a) hexane, (b) decane and octane, and (c) silicone oil *versus* oxygen treatment duration. (d) Illustrative comparison of the water drop morphology on pristine NWF and superhydrophobic-treated NWF after low-surface-energy liquid deposition. Water drops in tilted view on (e) the pristine NWF and (f) the superhydrophobic NWF, which are pre-wetted by hexane (dyed in blue).

contact angle to about 130°. These results indicate that the superhydrophobic-treated NWF can maintain strong water repellency even after wetting of hexane.

The above result is attributed to nanohairs on the fibers which facilitate the imbibitions of hexane into the fiber network so that only a very thin hydrocarbon film may remain on the fiber surface. See the illustration of Fig. 6(d). Nanohairs taller than the hydrocarbon film thickness are exposed to the atmosphere and thus can support a water droplet, leading to the recovery of strong water repellency. The difference of recovery behavior of hydrophobicity depending on the volume of hexane can be explained along the same line. The smaller the volume is, the thinner the hexane film. Therefore, nanohairs of AR = 17 and 49, corresponding to oxygen plasma treatment duration of 30 min and 60 min, respectively, can stick out of the film when hexane volume is 10 μl and 20 μl, respectively. When the nanohair AR is not high enough to be completely exposed to the atmosphere (corresponding to short plasma treatment duration or large hexane volume), the extent of contact angle recovery is limited so that the contact angle reaches about 130°.

It is not clearly known why the partially hexane-wetted nanohair structures of NWF exhibit a contact angle of 130° with water, although it is reasonably located between the contact angle of the dry superhydrophobic surface and the contact angle of water on hexane film. We see that this value is quite repeatedly obtained when different hydrocarbons, such as octane and decane, are pre-deposited on the

superhydrophobic-treated NWF as shown in Fig. 6(b). Again, pristine NWF exhibits a significant reduction of the contact angle with water after deposition of the hydrocarbons, but superhydrophobic NWFs treated with oxygen plasma and SiO_x–C:H coating sustain high contact angle of about 130° despite pre-wetting of the hydrocarbons.

We reproduce a similar tendency with nonvolatile silicone oils whose experimental results are shown in Fig. 6(c). Because of a high viscosity of silicone oil, which delays the spreading of oil into a thin film, the contact angle of NWFs with water remains low at about 100° when measured one hour after oil deposition for all the oxygen plasma treatment durations. It is noted that the contact angle of silicone oil film with a water drop is 90°, implying that the thick oil film efficiently blocks the contact of the nanohair structures with a water droplet. As we allow the silicone oil to spread into a thin film for a day so that nanohairs can contribute to the contact with water, the contact angle of superhydrophobic-treated NWF with water increases to about 130°, consistent with the foregoing results of the hydrocarbons.

Conclusions

We have developed a method to induce nanoscale roughness on NWFs of PET using oxygen plasma and lower its surface energy with HMDSO *via* rf-PECVD technique. Millimetre-sized water drops on the surface were shown to have a contact angle higher than 160° and the CAH less than 10°. In addition to this superhydrophobicity in a conventional measure, it is shown that thus-prepared surface can resist flooding due to high AR nanohairs with vapor condensation experiment in an ESEM chamber. This suggests a way to improve the resistance of functional materials, such as gas diffusion layer (GDL) of fuel cell membranes commonly made of carbon fiber,[54] to water flooding.

The superhydrophobic NWF is also demonstrated to sustain strong water repellency even after vapor condensation due to high AR nanohairs, which can help water drops to quickly roll off the surfaces. Although the plasma treated NWF is oleophilic, it maintains relatively strong water repellency owing to high AR nanohairs after low-surface-energy liquid wetting. This implies potential applications of the surface modification technology for the devices prone to oily contaminations, *e.g.* combustion engines and HVAC (heating, ventilation, and air conditioning) apparatus.

Acknowledgements

This work was supported by a grant from the Global Excellent Technology Innovation R&D Program funded by the Ministry of Knowledge Economy, Republic of Korea and a grant from KIST. HYK acknowledges administrative support from SNU-IAMD.

References

1 R. Furstner, W. Barthlott, C. Neinhuis and P. Walzel, *Langmuir*, 2005, **21**, 956–961.
2 L. Feng, S. H. Li, Y. S. Li, H. J. Li, L. J. Zhang, J. Zhai, Y. L. Song, B. Q. Liu, L. Jiang and D. B. Zhu, *Adv. Mater.*, 2002, **14**, 1857–1860.
3 Y. C. Jung and B. Bhushan, *Nanotechnology*, 2006, **17**, 4970–4980.
4 M. Miwa, A. Nakajima, A. Fujishima, K. Hashimoto and T. Watanabe, *Langmuir*, 2000, **16**, 5754–5760.
5 A. Nakajima, K. Hashimoto, T. Watanabe, K. Takai, G. Yamauchi and A. Fujishima, *Langmuir*, 2000, **16**, 7044–7047.
6 L. Jiang, Y. Zhao and J. Zhai, *Angew. Chem., Int. Ed.*, 2004, **43**, 4338–4341.
7 X. M. Li, D. Reinhoudt and M. Crego-Calama, *Chem. Soc. Rev.*, 2007, **36**, 1350–1368.
8 T.-G. Cha, J. W. Yi, M.-W. Moon, K.-R. Lee and H.-Y. Kim, *Langmuir*, 2010, **26**, 8319–8326.
9 H. Liu, L. Feng, J. Zhai, L. Jiang and D. B. Zhu, *Langmuir*, 2004, **20**, 5659–5661.
10 P. L. Chen, J. Y. Shiu, C. W. Kuo, P. L. Chen and C. Y. Mou, *Chem. Mater.*, 2004, **16**, 561–564.
11 H. Y. Erbil, A. L. Demirel, Y. Avci and O. Mert, *Science*, 2003, **299**, 1377–1380.
12 L. Feng, M. H. Jin, X. J. Feng, L. Feng, T. L. Sun, J. Zhai, T. J. Li and L. Jiang, *Adv. Mater.*, 2005, **17**, 1977–1981.
13 L. Feng, Y. A. Zhang, J. M. Xi, Y. Zhu, N. Wang, F. Xia and L. Jiang, *Langmuir*, 2008, **24**, 4114–4119.
14 H. Ji, M. H. Sun, C. X. Luo, L. P. Xu, H. Ji, O. Y. Qi, D. P. Yu and Y. Chen, *Langmuir*, 2005, **21**, 8978–8981.
15 K. K. S. Lau, J. Bico, K. B. K. Teo, M. Chhowalla, G. A. J. Amaratunga, W. I. Milne, G. H. McKinley and K. K. Gleason, *Nano Lett.*, 2003, **3**, 1701–1705.
16 L. Huang, S. P. Lau, H. Y. Yang, E. S. P. Leong, S. F. Yu and S. Prawer, *J. Phys. Chem. B*, 2005, **109**, 7746–7748.
17 W. Lee, M. K. Jin, W. C. Yoo and J. K. Lee, *Langmuir*, 2004, **20**, 7665–7669.
18 T. Onda, S. Shibuichi, N. Satoh and K. Tsujii, *Langmuir*, 1996, **12**, 2125–2127.
19 S. Michielsen and H. J. Lee, *Langmuir*, 2007, **23**, 6004–6010.
20 H. F. Hoefnagels, D. Wu, G. de With and W. Ming, *Langmuir*, 2007, **23**, 13158–13163.
21 J. Zimmermann, F. A. Reifler, G. Fortunato, L. C. Gerhardt and S. Seeger, *Adv. Funct. Mater.*, 2008, **18**, 3662–3669.
22 Z. M. Huang, Y. Z. Zhang, M. Kotaki and S. Ramakrishna, *Compos. Sci. Technol.*, 2003, **63**, 2223–2253.
23 M. Ma, M. Gupta, Z. Li, L. Zhai, K. K. Gleason, R. E. Cohen, M. F. Rubner and G. C. Rutledge, *Adv. Mater.*, 2007, **19**, 255–259.
24 B. Balu, V. Breedveld and D. W. Hess, *Langmuir*, 2008, **24**, 4785–4790.
25 K. Teshima, H. Sugimura, Y. Inoue, O. Takai and A. Takano, *Langmuir*, 2003, **19**, 10624–10627.
26 K. Teshima, H. Sugimura, Y. Inoue, O. Takai and A. Takano, *Chem. Vap. Deposition*, 2004, **10**, 295–297.
27 K. Teshima, H. Sugimura, Y. Inoue, O. Takai and A. Takano, *Appl. Surf. Sci.*, 2005, **244**, 619–622.
28 S. H. Li, S. B. Zhang and X. H. Wang, *Langmuir*, 2008, **24**, 5585–5590.
29 J. T. Tesfai, R. N. Perry and E. L. Jablonski, *J. Colloid Interface Sci.*, 2011, **354**, 895–899.
30 A. Ezzati, E. Gorouhi and T. Mohammadi, *Desalination*, 2005, **185**, 371–382.
31 A. Lafuma and D. Quéré, *Nat. Mater.*, 2003, **2**, 457–460.
32 Y. T. Cheng, D. E. Rodak, A. Angelopoulos and T. Gacek, *Appl. Phys. Lett.*, 2005, **87**, 194112.
33 K. A. Wier and T. J. McCarthy, *Langmuir*, 2006, **22**, 2433–2436.
34 R. D. Narhe and D. A. Beysens, *Europhys. Lett.*, 2006, **75**, 98–104.
35 C. H. Chen, Q. J. Cai, C. L. Tsai, C. L. Chen, G. Y. Xiong, Y. Yu and Z. F. Ren, *Appl. Phys. Lett.*, 2007, **90**, 173108.
36 J. B. Boreyko and C. H. Chen, *Phys. Rev. Lett.*, 2009, **103**, 174502.
37 L. Yin, Q. J. Wang, J. A. Xue, J. F. Ding and Q. M. Chen, *Chem. Lett.*, 2010, **39**, 816–817.
38 I. Woodward, W. C. E. Schofield, V. Roucoules and J. P. S. Badyal, *Langmuir*, 2003, **19**, 3432–3438.
39 Y. H. Yan, M. B. Chan-Park and C. Y. Yue, *Langmuir*, 2005, **21**, 8905–8912.
40 N. Vourdas, A. Tserepi and E. Gogolides, *Nanotechnology*, 2007, **18**, 125304.
41 J. Hopkins and J. P. S. Badyal, *Langmuir*, 1996, **12**, 3666–3670.
42 L. Li, Y. Li, S. Gao and N. Koshizaki, *J. Mater. Chem.*, 2009, **19**, 8366–8371.
43 L. Li, T. Zhai, H. Zeng, X. Fang, Y. Bando and D. Golberg, *J. Mater. Chem.*, 2011, **21**, 40–56.

44 H. M. Powell and J. J. Lannutti, *Langmuir*, 2003, **19**, 9071–9078.
45 K. K. Varanasi, M. Hsu, N. Bhate, W. S. Yang and T. Deng, *Appl. Phys. Lett.*, 2009, **95**, 094101.
46 K. Jiao and X. G. Li, *Int. J. Hydrogen Energy*, 2010, **35**, 9095–9103.
47 Y. X. Wang, S. Al Shakhshir and X. G. Li, *Appl. Energy*, 2011, **88**, 2168–2175.
48 Y. Zhao, Y. W. Tang, X. G. Wang and T. Lin, *Appl. Surf. Sci.*, 2010, **256**, 6736–6742.
49 M. Yu, G. T. Gu, W. D. Meng and F. L. Qing, *Appl. Surf. Sci.*, 2007, **253**, 3669–3673.
50 A. B. D. Cassie and S. Baxter, *Trans. Faraday Soc.*, 1944, **40**, 546–550.
51 R. N. Wenzel, *Ind. Eng. Chem.*, 1936, **28**, 988–994.
52 R. E. Johnson and R. H. Dettre, *J. Phys. Chem.*, 1964, **68**, 1744.
53 N. A. Patankar, *Langmuir*, 2004, **20**, 7097–7102.
54 C. Lim and C. Y. Wang, *Electrochim. Acta*, 2004, **49**, 4149–4156.